Propagative Oscillations in Codirectional Polariton Waveguide Couplers

J. Beierlein,[1,*] E. Rozas,[2] O. A. Egorov,[3] M. Klaas,[1] A. Yulin,[4] H. Suchomel,[1] T. H. Harder,[1] M. Emmerling,[1] M. D. Martín,[2] I. A. Shelykh,[4,5] C. Schneider,[1,6] U. Peschel,[3] L. Viña,[2,7,†] S. Höfling,[1,8] and S. Klembt[1,‡]

[1]*Technische Physik, Wilhelm-Conrad-Röntgen Research Center for Complex Material Systems, and Würzburg-Dresden Cluster of Excellence ct.qmat, Universität Würzburg, Am Hubland, D-97074 Würzburg, Germany*

[2]*Departamento de Física de Materiales, Instituto Nicolás Cabrera, Universidad Autónoma de Madrid, 28049 Madrid, Spain*

[3]*Institute of Condensed Matter Theory and Optics, Friedrich-Schiller-Universität Jena, Max-Wien-Platz 1, D-07743 Jena, Germany*

[4]*Faculty of Physics and Engineering, ITMO University, Saint Petersburg 197101, Russia*

[5]*Science Institute, University of Iceland, IS-107 Reykjavik, Iceland*

[6]*Institute of Physics, University of Oldenburg, D-26129 Oldenburg, Germany*

[7]*Instituto de Física de la Materia Condensada, Universidad Autónoma de Madrid, 28049 Madrid, Spain*

[8]*SUPA, School of Physics and Astronomy, University of St Andrews, St Andrews KY16 9SS, United Kingdom*

(Received 20 April 2020; accepted 8 January 2021; published 16 February 2021)

We report on novel exciton-polariton routing devices created to study and purposely guide light-matter particles in their condensate phase. In a codirectional coupling device, two waveguides are connected by a partially etched section that facilitates tunable coupling of the adjacent channels. This evanescent coupling of the two macroscopic wave functions in each waveguide reveals itself in real space oscillations of the condensate. This Josephson-like oscillation has only been observed in coupled polariton traps so far. Here, we report on a similar coupling behavior in a controllable, propagative waveguide-based design. By controlling the gap width, channel length, or propagation energy, the exit port of the polariton flow can be chosen. This codirectional polariton device is a passive and scalable coupler element that can serve in compact, next generation logic architectures.

DOI: 10.1103/PhysRevLett.126.075302

Photonic circuits rely on a variety of fiber-based optical elements for their functionality. These elements allow easy routing and filtering of signals. The main drawback of purely photonic schemes for logic operations, however, is a lack of self-interaction for very efficient switching [1,2]. The remarkable advances in exciton-polariton physics are a result of the progressing control of high-quality microcavities in which quantum well excitons and cavity photon modes couple strongly to form new hybrid light-matter eigenstates [3]. Polaritons exhibit a condensate regime at higher densities [4] with emission properties similar to those of a traditional laser without having to rely on population inversion [5]. This macroscopic quantum state [6,7] can propagate over macroscopic distances for high-quality samples [8]. Furthermore, polaritons can be excited and confined and therefore guided in waveguide structures [9]. Propitiously, the excitonic fraction of the polariton condensate is responsible for the observation of strong nonlinear interaction effects [10–12]. The photonic fraction allows for typical photonic benefits like a fast propagation velocity. Because of this interplay, a variety of next generation devices based on polaritons can be envisioned [13]. In particular, the possibility of using polaritons as information carriers in logic architectures has been addressed theoretically [14] and experimentally [15–22]. Recently, these ideas have been rekindled by related room temperature experiments using perovskites [23] and organic materials [24].

Basic routing effects have been predicted and achieved for polaritons [25,26], which show some functionality but are mainly based on active optical control. To this end, we demonstrate a new polariton device in a codirectional router, harnessing a Josephson-like oscillation effect in real space that could feasibly be scaled and does not need active external control. Josephson oscillations [27] occur when two quantum states are coupled by a transmissive barrier. They were first demonstrated in superconductors [28]. Similar effects have been observed in atomic Bose Einstein condensates [29–34] for which the interaction between the particles is crucial [35] to observe different interaction dependent regimes of coupling. For polaritons, this effect has first been observed in a naturally occurring disorder double potential well [36] and later in a dimer micropillar arrangement [37,38].

Our new coupler device consists of extended one-dimensional channels that allow observation of the oscillations in the spatial domain via a specifically tailored fabrication technique.

In this Letter, dedicated to a proof of concept, we use high-quality GaAs-based microcavities, benefiting from mature fabrication techniques [39]. For the codirectional couplers with waveguide coupling achieved by partially etched mirrors, we use molecular beam epitaxially grown microcavities hosting twelve GaAs quantum wells resulting in a Rabi splitting of 13.9 meV and a quality factor of $Q \approx 5000$ (see Supplemental Material [40] for further details). Sample processing was done via a specially developed reactive ion etching process. The first step consists of an electron beam exposure of a polymethyl methacrylate photoresist and subsequent development. Later, a metal layer of calibrated thickness is evaporated on the sampled followed by a lift-off process. After the lift-off process, the sample is etched. As a consequence of the protection by the predefined metal layers, the sample is only etched at the exposed positions. Due to the proximity of the structures and the anisotropic etching behavior of the reactive ion etching, the etching rate between the waveguides is slower, leaving a certain number of mirror pairs untouched. These left-over mirror pairs between the waveguides facilitate evanescent, photonic coupling. The area around the coupler is etched approximately halfway through the bottom distributed Bragg reflector and therefore facilitates strong photonic confinement.

Figure 1(a) shows a sketch of the intended structure, highlighting an excitation scheme (red), the incoupler region (orange), and the propagation direction x along the coupling area (blue). An SEM image of the full device and an enlarged view of the coupling region that stresses the fabrication-induced narrow gap between the structures are presented in Fig. 1(b) and (c), respectively. The incoupler, which is angled 45° to the propagation direction x [see Fig. 1(a)], has a width of 2 μm and a length of 40 μm. Figure 1(d) and (e) depict the energy dispersion of the ground state along the incoupler region in the linear regime and above the threshold, respectively. The calculated dispersion along the coupler is shown in Fig. 1(f).

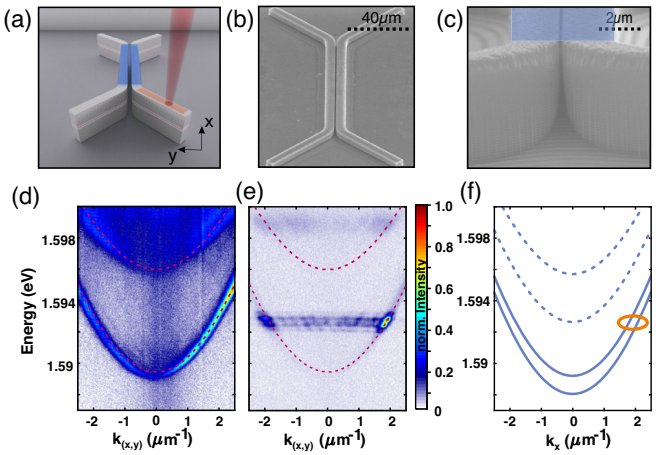

FIG. 1. Device layout, SEM images and corresponding experimental as well as theoretical dispersions of a codirectional coupler. (a) Device schematic with indicated laser excitation (red), incoupler region (orange), and the coupling region (blue) along the x axis. (b) Top view SEM image of a codirectional polariton coupler. (c) Enlargement highlighting the coupling region (blue) and the gap between the two waveguides. Here, the cavity and a varying number of mirror pairs are still intact. (d) Measured waveguide dispersion below and (e) above polariton condensation threshold at the input port region (orange) parallel to the waveguide, angled 45° to the x axis. (f) Calculated dispersion below the condensation threshold at the coupling region (blue).

The experiments have been carried out with two photoluminescence (PL) setups, the first capable of Fourier and real space emission detection while the second one was used for streak camera measurements. Excitation was provided using tuneable Ti:Sa lasers with 10 ps and 2 ps pulse lengths set at the wavelength of a high energetic Bragg minimum of the microcavity for each structure. The excitation was mechanically chopped with a ratio of 1:12 to prevent sample heating. Additionally, a tomography technique using motorized lenses was implemented to allow for energy selective imaging. The pump spot was focused via a microscope objective with NA = 0.42 to a diameter of $\sim$3 μm. As an example, we show the characterization of the incoupler with an excitation spot located at its center. The dispersion depicted in Fig. 1(d) was measured parallel to the incoupler at a low excitation density of 0.1 mW and fitted with an approach from Ref. [41]. This allows one to extract a detuning of -20 meV with an exciton energy of 1.609 eV. An investigation of the nonlinear regime in this structure is represented in Fig. 1(e), which shows polaritons above the threshold being expelled from the small laser pump spot [42] at a wave vector $k_x \approx 1.9\ \mu m^{-1}$. A detailed analysis of the emission intensity and energy as a function of the excitation power revealing a lasing threshold behavior and a continuous blueshift of 4 meV is presented in the Supplemental Material, confirming polariton interaction [43].

Let us now report on the main subject of the Letter, namely the oscillations in codirectional couplers. To this end, Fig. 2(a) depicts a logarithmic color-coded real space image of the energy-resolved PL from two adjacent waveguides at an injection power of 1 mW, corresponding to the propagating condensate regime for $E = 1.5924$–1.5930 eV. The gap between the two waveguides is 200 nm wide and the coupling area is 100 μm long. The emission from the region of the excitation spot (on the bottom left incoupler) is attenuated by a neutral density filter, while the far propagating condensate is amplified to compensate for its dissipative nature. A clear oscillation pattern is observed in the coupling region. In (b), the intensity distribution $\Delta I = (I_{top} - I_{bot})/I_{tot}$ between the two waveguides, where I_{top}, I_{bot}, and I_{tot} denote the intensities in the top, bottom, and top plus bottom waveguides, is presented. Therefore, $\Delta I = 0$ corresponds to an

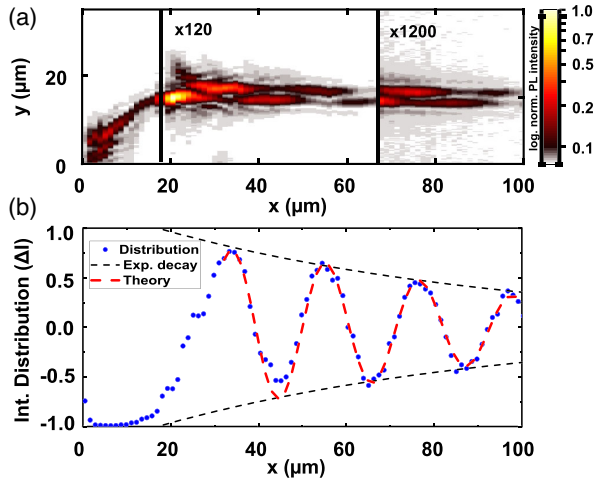

FIG. 2. Propagative oscillation of a exciton-polariton condensate in a codirectional coupler. (a) Energy-resolved real space PL for a coupler device with a gap size of 200 nm and a coupler region length of 100 μm at $E = 1.5924$–1.5930 eV. Polaritons are injected nonresonantly in the lower left incoupler and exhibit a distinct oscillatory behavior between the two waveguides in the coupler region (right of the black line). (b) Polariton PL distribution $\Delta I = (I_{\mathrm{top}} - I_{\mathrm{bot}})/I_{\mathrm{tot}}$. The red dashed line represents the results of the theoretical fitting by Eq. (5).

equal distribution of the population. Because of continuous polariton decay, we observe an exponential spatial decay $\tau_x = 80\ \mu\mathrm{m}^{-1}$. From Fig. 2(b), a spatial oscillation period of $\sim 20\ \mu$m is extracted.

The governing physics behind the observed oscillation dynamics can be understood within a slowly varying amplitude approach for the modes of the coupled waveguides. Since the excitation occurs above the condensation threshold, the ballistic polaritons have a well-defined frequency. Thus, we focus on spatial dynamics along the propagation axis x considering a monochromatic case. In the low-intensity limit, the dynamics can be modeled via two coupled equations for amplitudes $A_{1,2}$ in the coupled waveguides:

$$i\frac{\partial}{\partial x}A_1(x) = -\kappa A_1(x) - JA_2(x), \tag{1}$$

$$i\frac{\partial}{\partial x}A_2(x) = -\kappa A_2(x) - JA_1(x), \tag{2}$$

where $J \equiv J' + iJ''$ is the complex coupling constant that is governed by the width and depth of the gap between the coupled waveguides. The complex wave vector $\kappa = k + i\alpha$ characterizes the propagation and damping of guided modes in separated waveguides (in the following $\alpha > J'' > 0$).

In order to find the supermodes of the coupler, we look for a solution of Eqs. (1) and (2) in the form $A_{1,2}(x) = a_{1,2}\exp(i\beta x)$. By diagonalizing the system, one finds two eigenmodes, namely symmetric $a_1 = a_2$ and antisymmetric $a_1 = -a_2$, with the propagation constants $\beta_+ = \kappa + J' + iJ''$ and $\beta_- = \kappa - J' - iJ''$, respectively. It is worth mentioning that, due to the imaginary parts of the coupling constants, the damping rates $\mathrm{Im}(\beta_\pm) = \alpha \pm J''$ of these two modes are different. More precisely, the antisymmetric mode has smaller propagation losses. If only one waveguide is excited (with an amplitude A), the analytical solution for the mode dynamics can be easily found as

$$A_1(x) = Ae^{ikx-\alpha x} \times [\cos(J'x)\cosh(J''x) - i\sin(J'x)\sinh(J''x)], \tag{3}$$

$$A_2(x) = Ae^{ikx-\alpha x} \times [i\sin(J'x)\cosh(J''x) - \cos(J'x)\sinh(J''x)]. \tag{4}$$

From the analytical solution, Eqs. (3) and (4), it is easy to derive an expression for the intensity distribution in the coupler:

$$\Delta I = (I_1 - I_2)/I_{\mathrm{tot}} = \cos(2J'x)/\cosh(2J''x). \tag{5}$$

This solution has a form of damped oscillations where polaritons transfer between the two channels with a spatial period $\pi/J' = 21.36\ \mu$m and a damping coefficient given by the imaginary part of the coupling constant $2J'' = 0.021\ \mu\mathrm{m}^{-1}$ [see Fig. 2(b)]. It is worth mentioning, that, due to the etching of the Bragg mirror between two channels, the effect of local losses becomes comparable to the polariton tunneling dynamics, and thus the imaginary part of the coupling cannot be neglected. For a nonzero imaginary part $J'' > 0$, the symmetric mode decays faster and at propagation distances of the order of $1/J''$ and becomes much less intensive than the antisymmetric mode. This suppresses the mode beating at large propagation distances.

To underpin this rather qualitative analysis with a more thorough theoretical study, we performed numerical calculations in the frame of the mean-field model for 2D intracavity photons coupled strongly to the quantum well excitons [6,7].

Neglecting polarization effects, one obtains two coupled Schrödinger equations for the photonic field Ψ_C and coherent excitons Ψ_E given as

$$\partial_t\Psi_C - \frac{i\hbar}{2\mathrm{m_c}}\nabla^2_{x,y}\Psi_C + iV(x,y)\Psi_C + [\gamma_c - i(\omega_p - \delta)]\Psi_C = i\Omega_R\Psi_E + \Psi_C(x,y)e^{ik_p x}, \tag{6}$$

$$\partial_t\Psi_E - \frac{i\hbar}{2\mathrm{m_E}}\nabla^2_{x,y}\Psi_E + (\gamma_e - i\omega_p)\Psi_E = i\Omega_R\Psi_C. \tag{7}$$

The complex amplitudes are obtained through a standard averaging procedure of the related creation or annihilation operators. γ_c and γ_e denote the cavity photon damping and

dephasing rate of excitons, respectively. We note that, for cryogenic sample temperatures, the excitonic dephasing time can be comparable with the lifetime of intracavity photons. Thus, without loss of generality, they are assumed to be equal $\hbar\gamma_c = \hbar\gamma_e = 0.01$ meV. The effective photon mass in the planar region is given by $m_c = 36.13 \times 10^{-6}\ m_e$, where m_e is the free electron mass. The effective mass of excitons is $m_E \approx 10^5\ m_C$. Ω_R is the Rabi frequency that defines the Rabi splitting $2\hbar\Omega_R = 13.9$ meV. The photon-exciton detuning is given by the parameter $\hbar\delta = \hbar\omega_c - \hbar\omega_e = -20$ meV where ω_c is the cavity resonance frequency and ω_e is the excitonic resonance. Theoretical details regarding the chosen potential $V(x, y)$ and the excitation modeling can be found in the Supplemental Material.

Figure 3(a) and (b) show examples of oscillation dynamics for two slightly different frequencies of the wave packets. These oscillations are governed by interference of the symmetric and the antisymmetric modes of the coupler, which is clearly visible in the two-dimensional spectrum shown in the insets to Fig. 3. The insets in each panel represent the momentum space distribution of the propagating polaritons. The substantial difference in the period of spatial oscillations can be explained by a nonequidistant momentum splitting between the above mentioned symmetric and antisymmetric modes within the dispersion [see Fig. 1(f)]. Further examples in Fig. 3(c) and 3(d) show propagation dynamics in which the coupling strength is continuously weakened due to decreased wave function overlap via increased gap width. A clear change in the oscillation pattern is observed. Note that, due to pronounced dissipative effects within the gap between waveguides, the antisymmetric mode, which has the lowest overlap with the gap region, dominates the spectrum for larger gaps and, as a result, oscillations disappear [see Fig. 3(d)].

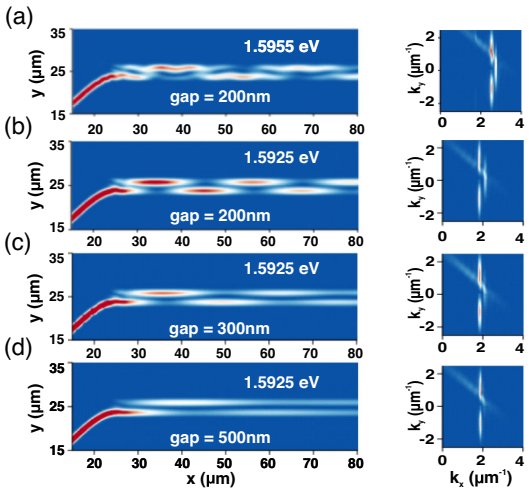

FIG. 3. Propagation dynamics of polaritons calculated within the model Eqs. (6) and (7) for coupled waveguides with separation gap sizes of (a),(b) 200 nm, (c) 300 nm, and (d) 500 nm. While the dynamics for (a) is at an energy of 1.5955 eV, (b)–(d) are at 1.5925 eV. The insets on the right-hand side show the respective distribution in momentum space (on the parameter plane k_y and k_x). Antisymmetric and symmetric modes of the coupler are visible.

Now, in order to demonstrate the polariton dynamics, we have performed energy- and time-resolved streak camera measurements using two devices with gap sizes of 200 nm and 500 nm. We use a streak camera with a time resolution of 10 ps. Because of the fast dynamics of polaritons in this sample, the polariton propagation is shown up to 30 ps here. The respective intensity patterns are plotted in Fig. 4(a)–(c) and (d)–(f).

In Fig. 4(a) at t = 0 ps, we observe the laser excitation spot on the lower left input coupler from where polaritons are repulsively expelled into the coupling region. At t = 12 ps, the polaritons have finished the first full oscillation. After approximately 30 ps, the polariton population has dissipated after a propagation length of 100 μm underlining the excellent quality of the patterned microcavity structure.

Fig. 4(d)–(f) show the temporal evolution in a system with a much larger gap of 500 nm. In this case, while there is some evanescent coupling to the upper waveguide, no pronounced oscillatory behavior is observed, again in excellent agreement with the theory presented in Fig. 3.

From the experiments as well as from the theoretical model, we can infer that a variation in the coupling strength ultimately allows for a change of the oscillation period. This can be used to choose the output port of the exciton-polariton flow due to a specifically tailored channel length and etch depth, similar to coupling behavior previously demonstrated for surface plasmon polaritons [44,45]. Figure 5 shows the results of the experiments. We have used similar couplers with 200 nm and 300 nm gap sizes, respectively, but with a reduced coupler region length of

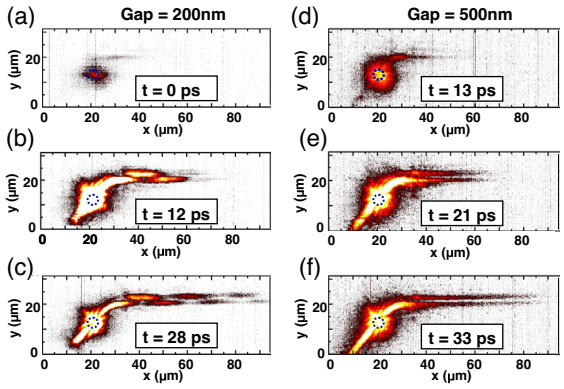

FIG. 4. Time-resolved propagation of the polariton propagation in coupler devices with a gap size of (a)–(c) 200 nm and (d)–(f) 500 nm for three different times during the propagation. While (a)–(c) show a clean oscillation between the two waveguides, no oscillation is visible in (d)–(f). The pump area is indicated by a blue dashed circle.

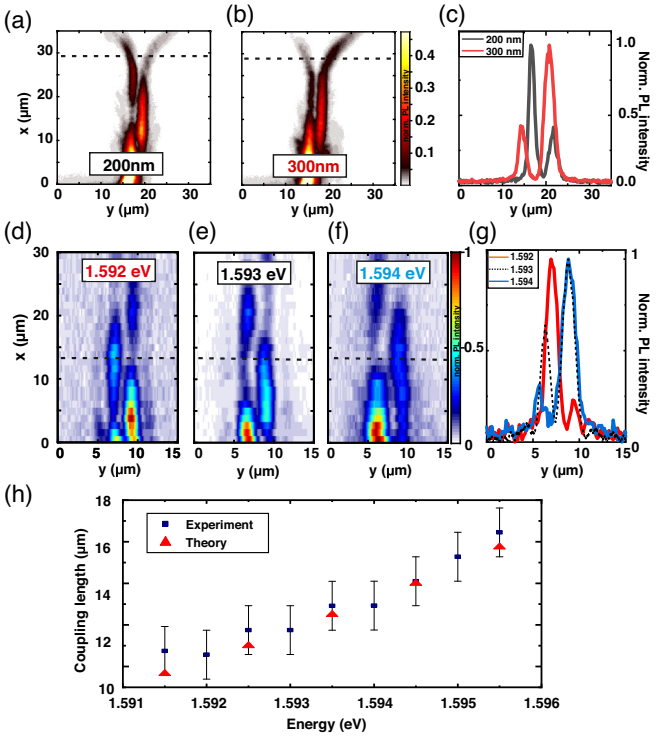

FIG. 5. Routing of a polariton condensate via a different coupling length (a)–(c) and different propagation energy (d)–(g). (Note that the plot orientation has been turned by 90° for visual clarity). A coupler with a length of the coupling region of 20 μm and a gap size of (a) 200 nm and (b) 300 nm is shown. (c) Line profiles of the normalized intensities at $x = 28$ μm for (a) and (b). The PL emission for different energies (d)–(f) in a fixed region of the coupler is shown. (g) Normalized PL intensity line profiles of the emission at $x = 13$ μm. (h) Experimentally extracted coupling lengths as a function of the propagation energy and numerically calculated values.

20 μm. While (a) shows the polariton flow leaving predominantly through the left outcoupler, the larger gap (weaker coupling and larger oscillation length) in (b) shows predominant coupling to the right arm. In (c) the normalized line profiles are plotted for Fig. 5(a),(b) at $x = 28$ μm. Another way of changing the output port is by changing the energy of the polariton condensate. The emissions of a condensate for three different energies ranging from $E =$ 1.592–1.594 eV are shown in Fig. 5(d)–(f). Changing the condensate propagation energy by 2 meV, a change of the intensity from left to right can be observed. This shift is underlined by the line profiles in Fig. 5(g). The detailed change of experimental coupling lengths, in excellent agreement with the numerically calculated values for Fig. 5(d)–(f), is depicted in Fig. 5(h).

Therefore, we have shown that this device configuration allows for codirectional routing to a predetermined exit port via a Josephson-like oscillation effect in real space.

In conclusion, we have demonstrated the possibility for passive polariton routing that is easily scalable and integratable to large polariton based logic networks. We evidenced this by a precise control of the lithographically engineered photonic landscape, which allows for the observation of these oscillations in real space between polaritonic waveguides. Such detailed tailoring of the flow of quantum fluids of light paves the way to harness their nonlinearity in next generation photonics. Furthermore, the basic understanding of the coupling of polariton waveguides [46,47] is the necessary foundation for larger coupled waveguide arrays comparable to those that have been implemented for the demonstration of topological waveguiding effects [48,49]. In this respect, our work opens a new route to use polariton waveguides for polariton logic as well as for topological devices involving nonlinearity, gain, interactions, and coherence inherent to the polariton system.

The Würzburg and Jena group acknowledges financial support within the DFG Projects No. SCHN1376/3-1, No. PE 523/18-1 and No. KL3124/2-1. The Würzburg Group acknowledges financial support by the German Research Foundation (DFG) under Germany's Excellence Strategy–EXC2147 "ct.qmat" (Project No. 390858490) and is grateful for support by the state of Bavaria. S. H. also acknowledges support by the EPSRC Hybrid Polaritonics grant (EP/M025330/1). The Würzburg group wants to thank Hugo Flayac for inspiring discussions in the early stage of this work. The Madrid group acknowledges financial support of the Spanish MINECO Grant No. MAT2017-83722-R. E. R. acknowledges financial support from a Spanish Formación Personal Investigador Scholarship No. BES-2015-074708. I. A. S. acknowledges the financial support of the Icelandic Science Foundation (project Hybrid polaritonics). I. A. S. and A. Y. acknowledge the Ministry of Science and Higher Education of the Russian Federation (Megagrant No. 14.Y26.31.0015).

J. B. and E. R. contributed to this work equally.

*Corresponding author.
johannes.beierlein@uni-wuerzburg.de
†Corresponding author.
luis.vina@uam.es
‡Corresponding author.
sebastian.klembt@physik.uni-wuerzburg.de

[1] D. A. B. Miller, Nat. Photonics **4**, 3 (2010).
[2] Z. Lu, H. Yun, Y. Wang, Z. Chen, F. Zhang, N. A. F. Jaeger, and L. Chrostowski, Opt. Express **23**, 3795 (2015).
[3] C. Weisbuch, M. Nishioka, A. Ishikawa, and Y. Arakawa, Phys. Rev. Lett. **69**, 3314 (1992).
[4] J. Kasprzak, M. Richard, S. Kundermann, A. Baas, P. Jeambrun, J. M. J. Keeling, F. M. Marchetti, M. H. Szymanska, R. Andre, J. L. Staehli, V. Savona, P. B. Littlewood, B. Deveaud, and L. S. Dang, Nature (London) **443**, 409 (2006).
[5] A. Imamoglu, R. J. Ram, S. Pau, and Y. Yamamoto, Phys. Rev. A **53**, 4250 (1996).

[6] I. Carusotto and C. Ciuti, Rev. Mod. Phys. **85**, 299 (2013).
[7] A. Amo, J. Lefrere, S. Pigeon, C. Adrados, C. Ciuti, I. Carusotto, R. Houdre, E. Giacobino, and A. Bramati, Nat. Phys. **5**, 805 (2009).
[8] B. Nelsen, G. Liu, M. Steger, D. W. Snoke, R. Balili, K. West, and L. Pfeiffer, Phys. Rev. X **3**, 041015 (2013).
[9] E. Wertz, A. Amo, D. D. Solnyshkov, L. Ferrier, T. C. H. Liew, D. Sanvitto, P. Senellart, I. Sagnes, A. Lemaître, A. V. Kavokin, G. Malpuech, and J. Bloch, Phys. Rev. Lett. **109**, 216404 (2012).
[10] M. Vladimirova, S. Cronenberger, D. Scalbert, K. V. Kavokin, A. Miard, A. Lemaître, J. Bloch, D. Solnyshkov, G. Malpuech, and A. V. Kavokin, Phys. Rev. B **82**, 075301 (2010).
[11] G. Muñoz-Matutano, A. Wood, M. Johnsson, X. Vidal, B. Q. Baragiola, A. Reinhard, A. Lemaître, J. Bloch, A. Amo, G. Nogues, B. Besga, M. Richard, and T. Volz, Nat. Mater. **18**, 213 (2019).
[12] A. Delteil, T. Fink, A. Schade, S. Höfling, C. Schneider, and A. Imamoglu, Nat. Mater. **18**, 219 (2019).
[13] D. Sanvitto and S. Kena-Cohen, Nat. Mater. **15**, 1061 (2016).
[14] T. C. H. Liew, A. V. Kavokin, and I. A. Shelykh, Phys. Rev. Lett. **101**, 016402 (2008).
[15] A. Amo, T. C. H. Liew, C. Adrados, R. Houdré, E. Giacobino, A. V. Kavokin, and A. Bramati, Nat. Photonics **4**, 361 (2010).
[16] C. Anton, T. C. H. Liew, G. Tosi, M. D. Martin, T. Gao, Z. Hatzopoulos, P. S. Eldridge, P. G. Savvidis, and L. Viña, Appl. Phys. Lett. **101**, 261116 (2012).
[17] T. Gao, P. S. Eldridge, T. C. H. Liew, S. I. Tsintzos, G. Stavrinidis, G. Deligeorgis, Z. Hatzopoulos, and P. G. Savvidis, Phys. Rev. B **85**, 235102 (2012).
[18] C. Anton, T. C. H. Liew, J. Cuadra, M. D. Martin, P. S. Eldridge, Z. Hatzopoulos, G. Stavrinidis, P. G. Savvidis, and L. Viña, Phys. Rev. B **88**, 245307 (2013).
[19] D. Ballarini, M. De Giorgi, E. Cancellieri, R. Houdré, E. Giacobino, R. Cingolani, A. Bramati, G. Gigli, and D. Sanvitto, Nat. Commun. **4**, 1778 (2013).
[20] H. S. Nguyen, D. Vishnevsky, C. Sturm, D. Tanese, D. Solnyshkov, E. Galopin, A. Lemaître, I. Sagnes, A. Amo, G. Malpuech, and J. Bloch, Phys. Rev. Lett. **110**, 236601 (2013).
[21] H. Suchomel, S. Brodbeck, T. C. H. Liew, M. Amthor, M. Klaas, S. Klembt, M. Kamp, S. Höfling, and C. Schneider, Sci. Rep. **7**, 5114 (2017).
[22] K. Winkler, H. Flayac, S. Klembt, A. Schade, D. Nevinskiy, M. Kamp, C. Schneider, and S. Höfling, Phys. Rev. B **95**, 201302(R) (2017).
[23] R. Su, J. Wang, J. Zhao, J. Xing, W. Zhao, C. Diederichs, T. C. H. Liew, and Qihua Xiong, Sci. Adv. **4**, eaau0244 (2018).
[24] A. V. Zasedatelev, A. V. Baranikov, D. Urbonas, F. Scafirimuto, U. Scherf, T. Stöferle, R. F. Mahrt, and P. G. Lagoudakis, Nat. Photonics **13**, 378 (2019).
[25] H. Flayac and I. G. Savenko, Appl. Phys. Lett. **103**, 201105 (2013).
[26] F. Marsault, H. S. Nguyen, D. Tanese, A. Lemaître, E. Galopin, I. Sagnes, A. Amo, and J. Bloch, Appl. Phys. Lett. **107**, 201115 (2015).
[27] B. Josephson, Phys. Lett. **1**, 251 (1962).
[28] P. W. Anderson, Rev. Mod. Phys. **38**, 298 (1966).
[29] F. S. Cataliotti, S. Burger, C. Fort, P. Maddaloni, F. Minardi, A. Trombettoni, A. Smerzi, and M. Inguscio, Science **293**, 843 (2001).
[30] M. Albiez, R. Gati, J. Foelling, S. Hunsmann, M. Cristiani, and M. K. Oberthaler, Phys. Rev. Lett. **95**, 010402 (2005).
[31] R. Gati, M. Albiez, J. Foelling, B. Hemmerling, and M. Oberthaler, Appl. Phys. B **82**, 207 (2006).
[32] R. Gati and M. K. Oberthaler, J. Phys. B **40**, R61 (2007).
[33] S. Levy, E. Lahoud, I. Shomroni, and J. Steinhauer, Nature (London) **449**, 579 (2007).
[34] A. Smerzi, S. Fantoni, S. Giovanazzi, and S. R. Shenoy, Phys. Rev. Lett. **79**, 4950 (1997).
[35] A. J. Leggett, Rev. Mod. Phys. **73**, 307 (2001).
[36] K. G. Lagoudakis, B. Pietka, M. Wouters, R. André, and B. Deveaud-Plédran, Phys. Rev. Lett. **105**, 120403 (2010).
[37] M. Abbarchi, A. Amo, V. G. Sala, D. D. Solnyshkov, H. Flayac, L. Ferrier, I. Sagnes, E. Galopin, A. Lemaître, G. Malpuech, and J. Bloch, Nat. Phys. **9**, 275 (2013).
[38] A. F. Adiyatullin, M. D. Anderson, H. Flayac, M. T. Portella-Oberli, F. Jabeen, C. Ouellet-Plamondon, G. C. Sallen, and B. Deveaud, Nat. Commun. **8**, 1329 (2017).
[39] C. Schneider, K. Winkler, M. D. Fraser, M. Kamp, Y. Yamamoto, E. A. Ostrovskaya, and S. Höfling, Rep. Prog. Phys. **80**, 016503 (2016).
[40] See Supplemental Material at http://link.aps.org/supplemental/10.1103/PhysRevLett.126.075302 for sample fabrication technique ,experimental and theoretical information on the photonic potential and the tuning of the oscillation.
[41] A. I. Tartakovskii, V. D. Kulakovskii, A. Forchel, and J. P. Reithmaier, Phys. Rev. B **57**, R6807 (1998).
[42] E. Wertz, L. Ferrier, D. D. Solnyshkov, R. Johne, D. Sanvitto, A. Lemaître, I. Sagnes, R. Grousson, A. V. Kavokin, P. Senellart, G. Malpuech, and J. Bloch, Nat. Phys. **6**, 860 (2010).
[43] C. Ciuti, V. Savona, C. Piermarocchi, A. Quattropani, and P. Schwendimann, Phys. Rev. B **58**, 7926 (1998).
[44] M.-Y. Pan, E.-H. Lin, L. Wang, and P.-K. Wei, Nanoscale Res. Lett. **9**, 430 (2014).
[45] Y. Zhang, Y. Xu, C. Tian, Q. Xu, X. Zhang, Y. Li, X. Zhang, J. Han, and W. Zhang, Photonics Res. **6**, 18 (2018).
[46] M. Klaas, J. Beierlein, E. Rozas, S. Klembt, H. Suchomel, T. H. Harder, K. Winkler, M. Emmerling, H. Flayac, M. D. Martin, L. Viña, S. Höfling, and C. Schneider, Appl. Phys. Lett. **114**, 061102 (2019).
[47] E. Rozas, J. Beierlein, A. Yulin, M. Klaas, H. Suchomel, O. Egorov, I. A. Shelykh, U. Peschel, C. Schneider, S. Klembt, S. Höfling, M. D. Martin, and L. Viña, Adv. Opt. Mater., **8**, 2000650 (2020).
[48] A. Blanco-Redondo, I. Andonegui, M. J. Collins, Gal Harari, Y. Lumer, M. C. Rechtsman, B. J. Eggleton, and M. Segev, Phys. Rev. Lett. **116**, 163901 (2016).
[49] S. Weimann, M. Kremer, Y. Plotnik, Y. Lumer, S. Nolte, K. G. Makris, M. Segev, M. C. Rechtsman, and A. Szameit, Nat. Mater. **16**, 433 (2017).